平成12年度プロジェクト報告書

Effects of HD Cooling on the Formation of the First Stars

Category B: Fumitaka Nakamura (nfn38 : nakamrfm)

Faculty of Education and Human Sciences, Niigata University, 8050 Ikarashi-2, Niigata 950-2181, Japan, and Astronomy Department, University of California, Berkeley, Berkeley, CA 94720

ABSTRACT

In the context of the star formation through the fragmentation of an extremely metal-deficient protogalactic cloud, the gravitational collapse of filamentary gas clouds is explored with the non-equilibrium chemistry of H_2 and HD. It is found by one-dimensional hydrodynamical simulations that the cloud evolution is prescribed mainly by the initial density (n_0) and H_2 abundance ($x_{H_2,0}$). In particular, it turns out that the evolution of low-density filaments (n_0 . 10^5 cm^{-3}) bifurcates at a critical H_2 abundance of $x_{H_2,cr} \simeq 3 \times 10^{-3}$, beyond which HD cooling overwhelms H_2 cooling. The contraction of a filament with n_0 . 10^5 cm^{-3} and x_{H_2} & $x_{H_2,cr}$ is strongly decelerated when the central density reaches a critical density of HD, and expected to fragment at the density of $\sim 10^7$ cm^{-3}. Then, the fragment mass is assessed to be $\approx 10 M_\odot$. Contrastingly, the contraction of a filaments with n_0 . 10^5 cm^{-3} but x_{H_2} . $x_{H_2,cr}$ is regulated by H_2 cooling. In this case, the filament tends to fragment at lower density as 10^{4-5} cm^{-3} owing to the low critical density of H_2, and the fragment mass is as high as $\approx 10^2 M_\odot$. As for high density filaments with n_0 & 10^5 cm^{-3}, the temperature stays at a relatively high value because both H_2 and HD cooling is saturated, and therefore HD does not play a significant role for the thermal evolution. The contraction of such a high-density filament is accelerated by the effective three-body H_2 formation when the density reaches 10^{8-9} cm^{-3}. Then, the fragmentation is not expected to take place until the cloud becomes opaque to H_2 lines at the density of 10^{12-13} cm^{-3}, so that the fragment mass is reduced to $1-2$ M$_\odot$. As a result, the stellar initial mass function (IMF) is likely to be double-peaked and deficient in sub-solar mass stars, where the high mass peak is around $10 M_\odot$ or $10^2 M_\odot$, dependently on the initial density and H_2 abundance. If the gas in protogalactic clouds is photoionized by UV radiation or shock-heated, the H_2 abundance could exceed $x_{H_2,cr} \simeq 3 \times 10^{-3}$ by reactions of $H + e \rightarrow H^- + h\nu$ and $H + H^- \rightarrow H_2 + e$. Then, the high mass peak would be $O(10) M_\odot$.

1. Introduction

The first generation of stars, namely Population III stars, are thought to form from almost metal-free gas with metallicity of $\sim 10^{-10} Z_\odot$ (see e.g., Carr, Bond, & Arnett 1984; Carr 1994). Such Population III stars may have produced heavy elements at redshifts of z & 10. Recent observations

of quasar absorption spectra show that the metallic pollution of the intergalactic space is at a level of $10^{-3}Z_\odot$ (e.g., Cowie & Songaila 1998). Also, it is widely accepted that a significant portion of old halo stars in our Galaxy have metallicity lower than $10^{-3}Z_\odot$ (Beers, Preston, & Shectman 1992). In addition, there are found extremely metal-poor ($\approx 10^{-2}Z_\odot$) blue compact dwarf galaxies (Kunth & Sargent 1986; Pustilnik et al. 2001). Thus, the star formation in protogalaxies must have proceeded in very metal-deficient environments.

When the metallicity is lower than $Z \sim 10^{-2}Z_\odot$, the cooling by heavy elements is less effective than cooling by hydrogen and helium (e.g., Yoshii & Sabano 1980; Böhringer & Hensler 1989; Omukai 2000; Nishi & Tashiro 2000). Hence, the thermal property of such metal-deficient gas is essentially the same as that of the metal-free gas, in which primordial molecules are the most effective coolants at low temperatures of $T < 10^4$ K. Among the primordial molecules, the importance of hydrogen molecules (H_2) on the formation of Population III stars have been emphasized by many authors because they are the most abundant molecules in primordial gas (Nakamura & Umemura 1999a, 2001, hereafter Papers I and II, and references therein). In the absence of heavy elements or dust grains, H_2 can form mainly via the radiative association of H^- which forms by virtue of a small amount of residual electrons left over from the cosmic recombination. Even minor fraction of H_2 provides significant cooling through rotational and vibrational transitions which can lower the gas temperature down to a few hundred K and accordingly reduce the Jeans masses to stellar mass scales.

Deuterated hydrogen molecules (HD) are considered to be the second most abundant molecules in primordial gas during the post-recombination era (e.g., Galli & Palla 1998 and references therein). In spite of its low abundance ($[HD/H_2] \sim 10^{-3}$), HD provides significant cooling at low temperature gas because HD has higher radiative transition probabilities and lower excitation temperatures than H_2 because of its finite dipole moment. (The lowest rotational radiative transition probability is $A_{20} = 3 \times 10^{-11}$ s^{-1} for H_2 and $A_{10} = 5 \times 10^{-8}$ s^{-1} for HD.) Thus, HD cooling can lower the gas temperature down to $T \sim$ 100K (e.g., Puy & Signore 1997; Bougleux & Galli 1997; Galli & Palla 1998; Flower et al. 2000).

In the bottom-up scenarios like cold dark matter models, the first pregalactic objects should have collapsed at redshifts of $z \sim 10 - 10^2$ and have masses of $10^5 - 10^8$ M$_\odot$ (Tegmark et al. 1998; Fuller & Couchman 2000). Before the first pregalactic objects collapse, the H_2 abundances reach at most $10^{-6} - 10^{-5}$ at the post-recombination epoch. When such first objects are virialized, the gas temperature ascends up to $10^3 - 10^4$ K, depending upon the collapse redshift and the cloud mass. This enhances the H_2 formation rate and causes their abundance to rise from the initial value of $10^{-6} - 10^{-5}$ to a quasi-static equilibrium value of $10^{-4} - 10^{-3}$ before the three-body H_2 formation becomes effective. However, because of the low H_2 abundance, it is difficult to lower the temperature down to 100 K. Thus, the cloud evolution is basically determined by H_2 cooling rather than HD cooling (Nakamura & Umemura 1999b, 2000; see also Lepp & Shull 1984).

However, in some situations, the HD cooling plays an important role. The massive ones of the

first stars would evolve into supernovae. Ferrara (1998) showed that in dense shells formed behind supernova shocks, H_2 molecules form efficiently owing to recombination lags of free electrons (see also Shapiro & Kang 1987; Kang & Shapiro 1992). In such dense shells, H_2 abundances reach 6×10^{-3}, an order-of-magnitude higher than those of the first collapsed objects, and consequently the gas temperature decreases to 100 K. In such gas shells, HD cooling is expected to be more efficient than H_2 cooling and the subsequent star formation in such shocked shells could be regulated by HD cooling (Uehara & Inutsuka 2000; Machida, Fujimoto, & Nakamura 2001).

Another possibility is the star formation from photoionized gas. Corbelli, Galli, & Palla (1998) studied the effects of the UV background radiation on the thermal evolution of the protogalaxies. They found that there is a critical redshift of $z \sim 1-2$, above which the gas disks with surface densities $10^{20}\,\mathrm{cm}^{-2} \lesssim N_{\rm HI} \lesssim 10^{21}\,\mathrm{cm}^{-3}$ are gravitationally stable at $T \sim 10^4$ K. Below this redshift, the declined UV radiation is shielded by the gas disks where the formation of molecular hydrogen promotes a rapid transition toward the cold H I phase with $\sim 10^2$ K. In such environments, the H_2 abundance can reach 10^{-2} with the help of abundant free electrons by the UV radiation. Susa & Umemura (2000) also showed that when pregalactic clouds more massive than $10^{11} M_\odot$ collapse under UV background radiation at low redshift of $z \sim 5$, they can be shielded against external UV radiation in the course of their contraction and the temperature descends down to T . 100 K owing to the high H_2 abundance (& 10^{-3}). HD cooling is likely to be important for the star formation in these protogalactic systems. In this paper, we extensively examine the effects of the HD cooling on the formation of stars in protogalaxies, and elucidate the role of HD molecules for the stellar initial mass function (IMF) there.

Recent studies have revealed that the star formation in metal-deficient gas is considerably different from the present-day star formation (Abel et al. 1998; Bromm, Coppi, & Larson 1999; Abel, Bryan, & Norman 2000; Papers I and II). In Paper II, we studied the collapse and fragmentation of primordial filaments, taking into account the effects of H_2 cooling. It is found that there is a critical initial density, beyond which the collapse of the filament is appreciably accelerated owing to enhanced cooling by three-body H_2 formation. Thus, depending upon the initial density, there are two characteristic mass scales of the fragmentation of the primordial filaments ($\approx 1-2 M_\odot$ and $\approx 10^2 - 10^3 \mathrm{M}_\odot$), both of which are related to the microphysics of H_2. The former is consistent with the estimate by Uehara et al. (1996) and Paper I. The latter is consistent with the numerical results of Bromm et al. (1999) and Abel et al. (2000). Then, the IMF is expected to be bimodal with peaks of $1-2 M_\odot$ and $\approx 10^2 \mathrm{M}_\odot$. Thus, the IMF might be time-varying with galaxy evolution from early collapsing stages to the present day.

The time-varying IMF has been considered by many authors (e.g., Larson 1986; Zepf & Silk 1996; Larson 1998). Larson (1998) have discussed that the top-heavy IMF at the early epochs of galaxy formation can explain several observational features of galaxies which seem to be inconsistent with a universal IMF. For example, in metal-poor ($\sim 0.05 Z_\odot$) starburst galaxy M82, stars with masses above 25 $\mathrm{M}_\odot$ seem to contribute significantly to the metal enrichment, implying that the IMF may have been different from the universal IMF (Nakamura et al. 2001, Umeda & Nomoto

2001; see also Tsuru et al. 1997). The observed abundances of elliptical galaxies and clusters of galaxies also show several trends that can be accounted for with such IMFs (Worthey, Faber, & Gonzales 1992). Furthermore, the G-dwarf problem might be responsible for a variable IMF at the early epoch of galaxy formation (van den Bergh 1962; Vazdekis et al. 1996; Worthey, Dorman, & Jones 1996; Larson 1998). It is thus important to understand what determines the IMF in very metal-deficient gas.

This paper is organized as follows. In §2, we describe model and numerical methods which are basically the same as those of Paper II. Numerical results are presented in §3. In §4, implications for the IMF of Population III and metal-deficient stars are discussed.

2. Model and Numerical Methods

In Papers I and II, we studied the collapse and fragmentation of filamentary clouds, taking the H_2 cooling into account. In this paper, we examine the effects of HD cooling on the evolution of the filaments. Our numerical model and method are the same as those of Paper II except for the inclusion of deuterium chemistry. In the following, we briefly review our numerical model. See §2 of Paper II for more detail.

We deal with the following 14 species: e, H, H^+, H^-, H_2, H_2^+, He, He^+, He^{++}, D, D^+, D^-, HD, and HD^+. The mass fraction of He is set to 0.24 of the total mass for all the models calculated in this paper. The D abundance is set to 4×10^{-5} by number, which is consistent with recent observations of the deuterium Ly-α feature in the absorption spectra of high-redshift quasars (e.g., Tytler et al. 1996; O'Meara et al. 2000). The reaction rate coefficients for the deuterium chemistry are given in Table 1, while the rate coefficients for other speices are the same as those of Paper II.

We take into account the following thermal processes: (1) H cooling by radiative recombination, collisional ionization, and collisional excitation, (2) H_2 line cooling by rotational and vibrational transitions, (3) cooling by H_2 collisional dissociation, (4) heating by H_2 formation, and (5) HD line cooling by rotational transitions. The HD line cooling is computed by the same method as the H_2 line cooling described in Paper II, which includes the escape probability method in an optically-thick regime. For the collisional deexcitation rates for HD, we consider both H-HD and H_2-HD collisions, using analytical fits of Galli & Palla (1998) and Flower & Roueff (1999). The six rotational levels are taken into account.

We consider an infinitely long cylindrical gas cloud which is collapsing in the radial direction. The initial temperature and relative abundances are assumed to be spatially constant. The initial abundances of electron and D^+ are set to $x_e = 5 \times 10^{-5}$ and $x_{D+} = 1 \times 10^{-7}$, respectively, for all models. (As mentioned in Papers I and II, the numerical results do not depend sensitively upon x_e. The numerical results are also not sensitive to the initial value of x_{D+}.) At the initial state, the relative abundances of H^-, H_2^+, He^+, He^{++}, D^-, HD, and HD^+ are set to zero for simplicity. The abundances of other species are determined by the conservation of mass and charge.

The density is assumed to be uniform along the cylinder axis and the radial distribution is expressed as

$$\rho = \rho_0 \left(1 + r^2/R_0^2\right)^{-2} , \tag{1}$$

where $R_0 = \sqrt{2fkT_0/(\pi G \rho_0 \mu)}$ is the effective radius, ρ_0 is the central mass density, T_0 is the initial gas temperature, μ is the mean molecular weight, and f is the ratio of the gravitational force to the pressure force. When $f = 1$, the density distribution accords with that of an isothermal cylinder in hydrostatic equilibrium. When the filamentary cloud forms through gravitational fragmentation of a parent sheetlike cloud, f is expected to be ≈ 2 (see §2.2 of Paper I).

The radial infall velocity is given by

$$v_r = -v_0 r \left(R_0 + \sqrt{R_0^2 + r^2}\right)^{-1} , \tag{2}$$

where v_0 is constant and is set to the initial sound speed. We neglect the effects of dark matter because after virialization of the parent system, the local density of baryonic gas is likely to be higher than the background dark matter density owing to radiative cooling (e.g., Umemura 1993).

Then, the model is specified by four parameters: n_0, T_0, f, and the H_2 abundance $x_{H_2,0}$. It should be noted that a higher initial H_2 abundance can be translated to a higher initial ionization degree of a parent cloud. This is because when the initial ionization degree of the parent cloud is higher, the H_2 molecules form more efficiently via the reactions of $H + e \rightarrow H^- + h\nu$ and $H + H^- \rightarrow H_2 + e$.

In Paper II, we followed the collapse and fragmentation of the primordial filaments with one-dimensional and two-dimensional axisymmetric simulations. The numerical results of Paper II showed that the fragment masses derived from the two-dimensional simulations are in good agreement with the estimate based on one-dimensional simulations. Therefore, in this paper, we pursue one-dimensional simulations on the collapse of the filaments to estimate the fragment masses.

We calculated more than 1000 models by choosing the model parameters n_0, T_0, f, and $x_{H_2,0}$ as $\log_{10}(n_0/\mathrm{cm}^{-3}) = 1.00, 1.33, 1.67, 2.00, \ldots, 6.00$, $T_0 = 200$, 300, 400 K, $f = 1.5, 2.0, 2.5, \ldots, 6.0$, and $x_{H_2,0} = 1 \times 10^{-4}, 3 \times 10^{-4}, 6 \times 10^{-4}, 1 \times 10^{-3}, \ldots, 1 \times 10^{-2}$, respectively.

3. Numerical Results

In Papers I and II, we studied the gravitational fragmentation of the primordial filaments, taking H_2 cooling into account. The numerical results showed that there is a threshold density, beyond which the collapse is accelerated owing to effective cooling by three-body H_2 formation.

In this section, we reexamine the collapse of the filaments, taking into account the HD cooling as well as H_2 cooling. As shown below, there is a critical initial H_2 abundance, above which HD cooling predominantly regulates the cloud evolution. Also, it is found that the HD cooling does

not play an important role for high-density gas. Thus, the evolution of the primordial filaments is classified into three cases, depending upon the initial density and initial H_2 abundance; (1) low-density filaments with high H_2 abundance, (2) low-density filaments with low H_2 abundance, and (3) high-density filaments.

In the following, we first compare the HD cooling and H_2 cooling on the density-H_2 abundance diagram to clarify the importance of HD cooling. Next, we show the numerical results of one-dimensional simulations.

3.1. Critical H_2 Abundance

What is of great significance is that the HD cooling sensitively depends on the cloud density and H_2 abundance. In Figure 1, the HD cooling rate is compared with the H_2 cooling rate , where the abscissa and ordinate indicate the cloud density and the H_2 abundance, respectively. For simplicity, the HD abundance is taken to be proportional to the H_2 abundance as $x_{\rm HD}/x_{\rm H_2} = 1 \times 10^{-4}$. which is consistent with those of the models in §3.3 and 3.4. The solid lines show the contour curves of the HD-to-H_2 cooling ratio. Here, the gas temperatures are indicated by dashed lines, which are determined by the condition of $t_{\rm cool} = 2.5 t_{\rm frag}$, where $t_{\rm cool}$ is a cooling time and $t_{\rm frag}$ is a fragmentation time which is proportional to the free-fall time (see below for the definition). In the region above the thick solid curve, the HD cooling rate is larger than the H_2 cooling rate and the equilibrium temperature is lower than $\sim$ 100 K. The contribution of HD to the total cooling rate is largest at the density of 10^5 cm^{-3} which is almost comparable to the critical density of HD beyond which the rotational level populations achieve the LTE.

In this figure, an evolutionary path of a gravitationally collapsing cloud is nearly parallel to the abscissa because the H_2 abundance stays nearly constant during the contraction before the three-body reactions become important. If the cloud has the initial H_2 abundance lower than a threshold value of $x_{\rm H_2,cr} = 3 \times 10^{-3}$, the HD cooling does not play a significant role in the thermal evolution of the clouds during the contraction because $\Lambda_{\rm HD} < \Lambda_{\rm H_2}$. For the filaments with n_0 . 10^5 cm^{-3} and $x_{\rm H_2}$ & $x_{\rm H_2,cr}$, the evolutionary path enters into the region of $\Lambda_{\rm HD} > \Lambda_{\rm H_2}$ in the course of contraction even if H_2 cooling is more efficient than HD cooling at the early stages. As shown below, when the density exceeds 10^5 cm^{-3}, the contraction slows down because the rotational levels achieve the LTE, and thus the cooling efficiency is reduced, Then, the actual temperature stays below 100 K. Consequently, HD cooling continues to play an important role in the contraction until the cloud becomes opaque to the HD lines. On the other hand, for the filaments with n_0 & 10^5 cm^{-3} and $x_{\rm H_2}$ & $x_{\rm H_2,cr}$, the evolutionary path goes into the region of $\Lambda_{\rm HD} < \Lambda_{\rm H_2}$ even if $\Lambda_{\rm HD}$ is larger than $\Lambda_{\rm H_2}$ at the initial state. In other words, for the filaments with densities higher than n_0 & 10^5 cm^{-3}, the HD cooling does not play an important role in the thermal evolution of the gas. In summary, if the initial parameters of the filaments are in the gray region, the HD cooling plays an important role in the thermal evolution of the gas. Thus, the cloud contraction and fragmentation are anticipated to depend sensitively on the initial density and H_2 abundance.

3.2. Low-Density Filaments with high H_2 abundances (n_0 . $10^5 cm^{-3}$ and $x_{H_2,0}$ & 3×10^{-3})

As a typical example of this case, we show the evolution of the model with $n_0 = 10$ cm^{-3}, $T_0 = 200$ K, $f = 2$, and $x_{H_2,0} = 3 \times 10^{-3}$.

Figures 2a, 2b, 2c, and 2d show the time evolution of (a) the temperature, (b) H_2 (*solid line*) and HD (*dashed line*) abundances, and (c) total (*solid line*), H_2 (*dashed line*), and HD (*dotted line*) cooling rates, (d) the cooling time (*solid line*), the contraction time (*dashed line*), and the fragmentation time (*dotted line*), respectively, as a function of the central density [$n_c \equiv \rho_c/(\mu m_H)$]. The central density monotonously increases with time. Therefore, the abscissa corresponds to the evolution time. The contraction and cooling times are respectively defined as $t_{dyn} \equiv \rho/\dot{\rho}$ and $t_{cool} \equiv 3nkT/(2\Lambda)$. The fragmentation time t_{frag} is defined as 2.5 times the inverse of the growth rate of the fastest-growing mode (Nakamura, Hanawa, & Nakano 1993; see also §4 for the definition of the fragmentation time). In practice, a filament does not fragment in one-dimensional calculations. Therefore, t_{frag} should be regarded as a measure of the fragmentation epoch as well as the free-fall time.

At the early stages of the contraction, the H_2 cooling dominates HD cooling. Thus, the equilibrium temperature is lowered to $T \sim 100$ K owing to the high H_2 abundance. When the density reaches $n_c \sim 10^3$ cm^{-3}, the HD cooling becomes dominant and the temperature descends down to $T \sim 50$ K accordingly. This is because HD has a critical density higher than H_2. (The critical density of HD is equal to $n_{HD,cr} \sim 10^{4-5}$ cm^{-3}, while the critical one for H_2 is $n_{H_2,cr} \sim 10^{3-4}$ cm^{-3}. When the density exceeds $n_{H_2,cr}$ or $n_{HD,cr}$, the LTE populations are achieved for the rotational levels of H_2 or HD, respectively.)

When the density reaches $n_{H_2,cr}$, the H_2 cooling is saturated and then HD cooling becomes dominant as the density increases. When the HD cooling becomes effective, the equilibrium temperature descends to ~50 K owing to lower excitation temperatures of HD. Thereafter, the temperature stays nearly constant at ~50 K during the contraction. When the density reaches a critical density of HD, $n_{cr} \sim 10^{4-5}$ cm^{-3}, the cloud contraction tends to become quasistatic by the combination effect of (1) the dynamical stability of a *cylindrical* cloud and (2) the characteristic of line cooling. First, a polytropic cylinder ($P \propto \rho^\gamma$) in hydrostatic equilibrium is dynamically stable if the effective γ is greater than unity. This means that an isothermal cylinder is in the state of marginal stability. Second, at lower density than the critical density, the line cooling rate is nearly proportional to n^2 because the collisional excitation rate balances with spontaneous emission rate, while, at higher density than the critical density, the cooling rate is proportional to n because the level population achieves the Boltzmann distributions. Hence, t_{cool} is inversely proportional to the density for $n < n_{cr}$, while t_{cool} is constant for $n > n_{cr}$ if the temperature is constant. By these effects, the compressional heating strongly brakes the dynamic contraction when $n > n_{cr}$ and then the cloud evolves quasistatically. [In contrast, a spherical cloud is unstable if $\gamma < 4/3$. Therefore, the dynamical contraction is not decelerated even if the density exceeds the critical density (see Omukai

& Nishi 1998). Then, the temperature gradually increases and thus the HD cooling is less effective in a collapsing *spherical* cloud as shown by Lepp & Shull (1984). In this case, the evolutionay path of a gravitationally collapsing sphere will be reproduced by a $x_{H_2} \simeq$ constant line which is almost parallel to the abscissa in Figure 1.]

When the density reaches $\sim 10^9$ cm^{-3}, the cloud becomes optically thick to HD lines. Then, the quasistatic contraction almost ceases at that stage. However, as shown by two-dimensional calculations in Paper II, it is anticipated that the fragmentation takes place when the contraction time becomes a few times longer than the fragmentation time (see Paper II for more detail). Thus, this cloud is expected to undergo the fragmentation when the density reaches 10^7 cm^{-3}.

Uehara & Inutsuka (2000) estimated the minimum fragment mass at the stage optically thick to HD lines. However, in their model, the cloud becomes optically thick to HD lines when the density reaches $\approx 3 \times 10^{10}$ cm^{-3}, which is about 30 times higher than the present result. To see this discrepancy in detail, we compare our evaluation of the optical depth with the LVG approximation (Goldreich & Kwan 1974) with some modification. The optical depth of the LVG approximation is originally given by

$$\tau_{J+1,J} = \frac{hc}{4\pi} \frac{B_{J,J+1} n_J}{|dv/ds|} \left(1 - \frac{g_J n_{J+1}}{g_{J+1} n_J} \right) , \tag{3}$$

where h is the Plank constant, c is the speed of light, $B_{J,J+1}$ is Einstein's B coefficient of the transition $J \rightarrow J+1$, $|dv/ds|$ is the velocity gradient, n_J and g_J are the number density and the Gaunt factor of the J level, respectively. However, in the present calculations, the velocity gradient is small compared to the thermal width and the gradient of thermal velocity is dominant. Hence, we replace the velocity gradient by $\alpha v_{\rm th}/R_{\rm J} = \alpha\sqrt{\pi G \rho_0}$, where α, $v_{\rm th}$, and $R_{\rm J}$ are the nondimensional numerical constant, the thermal velocity, and the filament radius, respectively. If we set the temperature to 60 K, the optical depth of the most effective cooling line ($J = 1 \rightarrow 0$) becomes unity when the density reaches $1 - 3 \times 10^9$ cm^{-3} for $\alpha = 1 - 2$. This is consistent with the present result. Also, it should be noted that our definition of the fragment mass is different from that of Uehara & Inutsuka (2000). We adopt the mass contained within one wavelength of the fastest-growing linear perturbation which is consistent with our two-dimensional numerical results (see §4), while Uehara & Inutsuka (2000) adopted the Jeans mass which is about ten times smaller than our definition at the same density and temperature. As a result, their estimation of fragments due to HD cooling is by about two orders of magnitude smaller than our estimate if we assume the cloud to fragment at the stage optically thick to HD lines. But, in practice, the cloud is likely to fragment at earlier stages around the critical density of HD molecules as shown above.

The evolution of the other models with different initial parameters (10 cm^{-3} . n_0 . 10^4 cm^{-3}, 200 K . T_0 . 400 K, 1.5 . f . 6, and 3×10^{-3} . $x_{H_2,0}$. 10^{-2}) is qualitatively similar to that of the model shown in Figure 2. When the initial H_2 abundance is as high as 10^{-2}, the HD cooling is more effective than H_2 cooling at the initial state. Thus, the temperature goes down to ~ 50 K at the very early stages of the evolution.

3.3. Low-Density Filaments with Low H_2 Abundances ($x_{H_2,0}$. 3×10^{-3})

As a typical example of this case, we show the evolution of the model with $n_0 = 10$ cm^{-3}, $T_0 = 400$ K, $f = 2$, and $x_{H_2,0} = 1 \times 10^{-4}$.

Figure 3 shows the time evolution of this model as a function of the central density. The notation of the figure is the same as that of Figure 2. (The evolution is quite similar to that of Figure 1 of Paper II.) In this model, the cooling rate by HD is smaller than that by H_2 during the contraction. In other words, HD cooling does not play a significant role in the thermal and dynamical evolution. The temperature is kept between 100 and 500 K over 11 orders of density until the H_2 lines become optically thick. The abundances of H_2 and HD stay nearly constant at $x_{H_2} \sim 10^{-3}$ and $x_{HD} \sim 10^{-7}$ until the central density reaches 10^8 cm^{-3}. During the contraction, the HD abundance is nearly proportional to that of H_2 ($x_{HD} \sim 10^{-4} x_{H_2}$) because HD molecules form primarily via the reaction $D + H_2 \rightarrow H + HD$ in this model. Thus, when the three-body H_2 formation becomes effective, almost all the D atoms are processed into HD. It should be noted that the above reaction is sensitive to the temperature, and for lower temperature, the reactions $D^+ + H_2 \rightarrow H^+ + HD$ and $HD^+ + H \rightarrow D^+ + HD$ are more effective.

The contraction proceeds quasi-statically after the density reaches the critical density of H_2 ($n > n_{H_2,cr} = 10^{3-4}$ cm^{-3}). When the three-body H_2 formation becomes effective, the radial contraction is accelerated again until the cloud becomes optically thick to the H_2 lines ($n \sim 10^{12}$ cm^{-3}). The contraction is decelerated when the H_2 lines become optically thick ($\sim 10^{12}$ cm^{-3}). The cloud is expected to fragment after the density reaches the critical density of H_2.

The evolution of the other models with different parameters (10 cm^{-3} . n_0 . 10^4 cm^{-3}, 200 K . T . 400 K, 1.5 . f . 6, and 10^{-4} . $x_{H_2,0}$. 10^{-3}) is qualitatively similar to that of this model.

3.4. High-Density Filaments

As a typical example of this case, we show the evolution of the model with $n_0 = 10^6$ cm^{-3}, $T_0 = 200$ K, $f = 6$, and $x_{H_2,0} = 1 \times 10^{-2}$.

Figure 4 shows the time evolution of this model as a function of the central density. The notation of the figure is the same as that of Figure 2. Although the initial H_2 abundance is as high as 10^{-2}, the evolution is essentially the same as those of the models with low initial H_2 abundances (see §3.2 of Paper II). Since the initial density is higher than the critical densities of H_2 and HD, the temperature increases as the collapse proceeds. Therefore, even if at the initial state, HD cooling is more effective than H_2 cooling, H_2 cooling becomes dominant as the collapse proceeds. In other words, HD cooling does not play a significant role in the contraction of the dense filaments. Thus, the evolution is essentially the same as that without HD cooling.

The contraction time does not become longer than the fragmentation time until the H_2 lines become optically thick ($n_c \sim 10^{12} - 10^{13}$ cm^{-3}). This comes from the rapid increase in the H_2 abundance due to the effective three-body reaction. Therefore, the fragmentation is not expected to take place until the cloud becomes opaque to the H_2 lines. The fragment mass is assessed in the next section.

The evolution of the other models with different parameters (n_0 & 10^5 cm^{-3}, 200 K . T . 400 K, $2-3$. f . 6, and 10^{-4} . $x_{H_2,0}$. 10^{-3}) is qualitatively similar to that of this model.

4. Dependence of the Fragment Mass on the Initial Model Parameters

In this section, we estimate the fragment mass with the one-dimensional numerical results obtained in the previous section. As shown in the previous section, there is a threshold H_2 abundance, beyond which HD cooling can play a key role in the thermal evolution of primordial gas clouds, and also there is a threshold initial density, below which the filament would fragment at the critical density of H_2 or HD. Hence, as anticipated from the above numerical results, the fragment mass is also divided into three cases, depending upon the initial H_2 abundance and density.

In Paper II, we obtained the typical fragment masses with two-dimensional simulations. Comparing one-dimensional results with two-dimensional results, we found that the fragmentation takes place when $t_{\rm dyn}$ reaches $2-3t_{\rm frag}$ in the presence of small perturbations. We thus assume that a filament fragments into dense cores when the dynamical time reaches 2.5 times the fragmentation time, $t_{\rm dyn} = 2.5t_{\rm frag}$. The fragment masses are computed as $M_{\rm frag} \equiv m_{\rm eff}\lambda$, where $m_{\rm eff} = \int 2\pi r\rho dr$ is a line mass which is obtained by integrating the density from the center to the radius at which the density takes $0.1n_c$ and λ is a longitudinal wavelength of a fastest-growing linear perturbation (eq.[38] of Nakamura et al. 1993). This mass is about ten times larger than the Jeans mass.

Figures 5a and 5b show the distributions of the fragment mass derived from the one-dimensional simulations for the models with $x_{H_2,0} = 1 \times 10^{-3}$ and 3×10^{-3}, respectively. The abscissa and ordinate denote the initial central density and the parameter f, respectively. The solid lines denote the contours of the fragment mass which are labeled with adjacent numbers. The dashed lines show the lines at which the HD cooling rate is equal to H_2 cooling rate at the epoch of fragmentation. In the left regions of the dashed lines, HD cooling is more efficient than H_2 cooling. As mentioned above, there is a threshold value of the initial H_2 abundance, above which the HD cooling significantly affects the distribution of the fragment masses ($x_{H_2,\rm cr} = 3 \times 10^{-3}$ for $x_{\rm D} = 4 \times 10^{-5}$).

For the models with $x_{H_2,0} < x_{H_2,\rm cr} \approx 3 \times 10^{-3}$ (Figures 5a), the mass distribution of the fragments is quite similar to the case without HD (Paper II), because HD cooling does not play an important role in the thermal evolution of the filaments. For higher initial density and/or larger f, the fragment mass is lower. The maximum and minimum masses are estimated as $\sim 10^3 M_\odot$ and $1-2M_\odot$, respectively. (The maximum mass is a few times smaller than that of Paper II because of the higher initial H_2 abundance. For the models with $x_{H_2,0} = 1 \times 10^{-4}$, the mass distribution

as well as the maximum mass is in good agreement with that of Paper II.) As addressed in Paper II, these masses are related to the microphysics of H_2. The former corresponds to the Jeans mass at the stage at which the density reaches a critical density of H_2 beyond which the contraction becomes quasistatic. The latter corresponds to the Jeans mass at the stage at which the cloud becomes opaque to the H_2 lines and the contraction is appreciably decelerated.

There is a steep boundary at $n \sim 10^4 - 10^5$ cm^{-3} in the mass distribution of the fragments for $f \gtrsim 3$. For the models with $n_0 \gtrsim 10^5$ cm^{-3}, the fragment masses take their minima at $1 \sim 2$ M$_\odot$, whereas, for the models with $n_0 \lesssim 10^5$ cm^{-3}, they are greater than $\sim 10^2$ M$_\odot$. This sensitivity in the fragment mass comes from the rapid increase in H_2 abundance due to the three-body reactions. For the models with low densities ($n_0 \lesssim 10^5$ cm^{-3}), the contraction becomes quasistatic when the density reaches the critical density of H_2 and then linear density fluctuations can grow nonlinearly before the three-body H_2 formation becomes dominant ($n_0 \gtrsim 10^{8-9}$ cm^{-3}). In contrast, for the models with high densities ($n_0 \gtrsim 10^{5-6}$ cm^{-3}), the contraction time does not exceed the fragmentation time until the H_2 lines becomes optically thick at $n \sim 10^{12} - 10^{13}$ cm^{-3}.

On the other hand, when the initial H_2 abundance is higher than 3×10^{-3}, the HD cooling is more effective than the H_2 cooling for low-density filaments. Thus, the maximum mass of low-density region reduces to a few tens M$_\odot$ (The fragment mass depends weakly upon the initial H_2 abundance. For example, for the models with $x_{H_2,0} = 1 \times 10^{-2}$, the fragment mass is around 10 M$_\odot$ in the low-density region.). The reduced maximum mass is then related to the Jeans mass at the stage at which the density reaches a critical density of HD. The minimum mass does not change because HD is not a dominant coolant in the evolution of dense filaments. Therefore, similarly to the models with low H_2 abundance, the dependence of the fragment mass on the initial density exhibits a steep boundary around $n_0 = 10^4 - 10^5$ cm^{-3} for $f \gtrsim 3$.

In summary, the distributions of the fragment mass formed from very metal-poor gas clouds has a steep boundary around $n_0 \gtrsim 10^{4-5}$ cm^{-3} for $f \gtrsim 3$, irrespectively of the initial H_2 abundance. This implies that the IMFs in very metal-deficient gas are likely to be bimodal if both low-density and high-density filaments bear stars. The low-mass peak is around a few $M_\odot$, which is not sensitive to the abundance of H_2 formed in a parent cloud. The high-mass peak is $\approx 10^2 M_\odot$ if the initial H_2 abundance is lower than 3×10^{-3}, while it is $\approx 10 M_\odot$ if the initial H_2 abundance is higher than 3×10^{-3}. In the next section, we discuss some implications of such bimodal IMF in the very metal-deficient gas.

5. Discussion

As shown above, the distributions of the fragment mass are sensitive to the initial H_2 abundance. The initial H_2 abundance of filaments can be translated to the ionization degree of a parent cloud. When the initial ionization degree is higher, the H_2 molecules form more efficiently via gas-phase reactions of $H + e \rightarrow H^- + h\nu$ and $H + H^- \rightarrow H_2 + e$. Therefore, higher initial H_2 abundances

correspond to higher initial ionization degree of the parent cloud which is likely to be determined by intergalactic environments such as UV radiation and shocks which can ionize the gas. This implies that the the fragmentation process depends strongly on the intergalactic environments. In the following, we attempt to apply our numerical results to the star formation in very metal-poor environments.

5.1. Implications for the IMF of the Very First Stars

In the bottom-up scenarios like cold dark matter models, the first pregalactic objects should have collapsed at redshifts of $z \sim 10 - 10^2$ and have masses of $10^5 - 10^8$ $M_\odot$ (Tegmark et al. 1998; Fuller & Couchman 2000). When such first objects are virialized, the H_2 abundance reaches at most $10^{-4} - 10^{-3}$ which is lower than the threshold H_2 abundance of 3×10^{-3}. Therefore, HD cooling is not important to the formation of the very first stars (Nakamura & Umemura 1999b, 2000).

If more massive pregalactic objects collapse at high redshifts, the gas is highly ionized at the virialization epoch. Then, H_2 abundances may exceed the critical value. However, CDM models claim that such massive objects collapse preferentially at lower redshifts at which the universe would be already reionized and the intergalactic environments would be significantly changed. Such massive objects would be rare at high redshifts of $z \gtrsim 10$ and would not contribute to the formation of the very first stars. Furthermore, if such clouds collapse at redshifts of $z \gtrsim 20$, their temperature would be regulated by CMB temperature.

In summary, HD cooling does not play a significant role in the formation of the very first stars. Then, the IMF of the very first stars is predicted to be bimodal with peaks of $1 - 2M_\odot$ and $\approx 10^2 M_\odot$ if the dependence of fragment mass upon the initial density is translated into the dependence on local amplitude of random Gaussian density fields or the collapse epoch of a parent cloud. (Here, we assume that the stellar masses are almost comparable to those of the fragment masses.) See §5 of Paper II for more detail.

If primordial D abundance is a few times as high as the value we assumed in this paper ($x_D = 4 \times 10^{-5}$), HD cooling may play a role in the thermal evolution of the pregalactic clouds. However, recent observations of quasar absorption spectra have suggested that observed primordial D abundance is as low as $3 - 4 \times 10^{-5}$ (Tytler et al. 1996). Inhomogenious big bang nucleosynthesis might make primordial D abundance higher in some clouds, in which HD could play a key role in the formation of the very first stars.

5.2. Implications for Galaxy Formation

In this subsection, we apply our results to early stages of galaxy formation at which metallicity is expected to be very low.

Recently, Susa & Umemura (2000) investigated the pancake collapse of pregalactic clouds under UV background radiation. They found that once the pancaking disk is shielded against external UV radiation in the course of contraction, the H_2 molecules form efficiently via H^- reaction with abundant free electrons produced by UV background, and the resultant abundance reaches $x_{H_2} \approx 3\times10^{-3}$ (see also Shapiro & Kang 1986). The pancake disks probably fragment into filaments in which stars would form. In this case, HD cooling is expected to become efficient in low-density filaments and then, the high mass peak of the IMF would go down to $\sim 10\ M_\odot$.

It is found that at redshifts of $z \sim 2$, the UV background radiation decreases with time (Irwin, McMahon, & Hazard 1991; Maloney 1993; Henry & Murthy 1993; Dove & Shull 1994). The time-decreasing UV background radiation is also likely to influence star formation in galaxies, especially dwarf galaxies with low surface densities which may be related to excess number count of faint blue objects observed in the Hubble Deep Field (e.g., Ellis 1997). Corbelli, Galli, & Palla (1998) studied the effects of the declined UV background radiation on the thermal evolution of the protogalaxies with low surface densities. They found that there is a critical redshift of $z \sim 1-2$, above which the gas disks with surface densities $10^{20}\ \mathrm{cm}^{-2} \lesssim N_{\mathrm{HI}} \lesssim 10^{21}\ \mathrm{cm}^{-3}$ are gravitationally stable at $T \sim 10^4$ K. Below this redshift, the declined UV radiation is shielded by the gas disks where the H_2 abundance reaches 10^{-2} owing to high ionization degree by the UV radiation. The enhanced H_2 formation promotes a rapid transition toward the cold H I phase with $\sim 10^2$ K. Thus, in such dwarf galaxies, high mass peak of the IMF would decrease to $\sim 10\ M_\odot$ owing to HD cooling. Based on X-ray observations of a starburst metal-poor galaxy M82, stars with masses above $25\ M_\odot$ seem to contribute significantly to the metal enrichment of the galaxy (Tsuru et al. 1997; Nakamura et al. 2001; Umeda & Nomoto 2001). This mass scale seems to be consistent with the high mass peak of the present IMF regulated by HD cooling. The high mass peak of our IMF is also consistent with the estimate by Hernandez & Ferrara (2001).

If the high-mass component of the IMF contributes significantly to the early metal enrichment of galaxies, the abundance ratio would be different from that in interstellar medium around Population I stars. In fact, the observations of hot gas in giant ellipticals and clusters of galaxies have shown that the abundance ratios of α elements to iron are higher than those expected from the Salpeter IMF (Worthey et al. 1996; Loewenstein & Mushotzky 1996). Such a trend seems to be consistent with the high contribution of massive stars to the metal enrichment at the early epochs.

As the star formation progresses, the metallicity of the interstellar gas will monotonously increase with time. When the metallicity reaches $10^{-3} - 10^{-2} Z_\odot$, the metal cooling becomes important and the thermal properties of the gas are changed. Thereafter, the process of star formation would become similar to that of the present-day star formation. In other words, the IMF would settle into Salpeter-like IMF.

We are grateful to A. Ferrara, T. Nakamoto, R. Nishi, K. Omukai, H. Susa, and H. Uehara for stimulating discussion. Numerical computations in this work were carried out on VPP300/16R and VX/4R at the Astronomical Data Analysis Center of the National Astronomical Observatory, Japan and on workstations at the Center for Computational Physics, University of Tsukuba. This work was financially supported in part by the Grant-in-Aid for Scientific Research on Priority Areas of the Ministry of Education, Science, Sports and Culture 10147205 and 11134203 (FN).

REFERENCES

Abel, T., Anninos, P. A., Norman, M. L., & Zhang, Y. 1998, ApJ, 508, 518

Abel, T., Bryan, G. L., & Norman, M. L. ApJ, 540, 39

Audouze, J., & Silk, J. 1995, ApJ, 451, L49

Beers, T. C., Preston, G. W., & Shectman, S. A. 1992, AJ, 103, 1987

Böhringer & Hensler, 1989, ApJ, 215, 147

Bougleux, E., Galli, D., 1997, MNRAS, 638, 648

Bromm, V., Coppi, P. S., Larson, R. B. 1999, ApJ, 527, L5

Carr, B. J., Bond, J. R., & Arnett, W. D. 1984, ApJ, 277, 445

Carr, B. J. 1994, ARA&A, 32, 531

Chabrier, G., Segretain, L. & Mera, D. 1996, ApJ, 468, L21

Chabrier, G. 1999, ApJ, 513, 103

Coppi, P. S., Bromm, V., & Larson, R. B. 2001, in The Physics of Galaxy Formation, p. 15

Corbelli, E., Galli, D., & Palla, F. 1997, ApJ, 487, L53

Couchman, H. M. P., & Rees, M. J. 1986, MNRAS, 221, 53

Cowie, L. L., & Songaila, A. 1998, Nature, 394, 44

Dove, J. B., & Shull, M. 1994, ApJ, 423, 196

Ellis, R. S. 1997, ARA&A, 35, 389

Ferrara, A. 1998, ApJ, 499, L17

Flower, D. R. 2000, MNRAS, 318, 875

Flower, D. R., Le Bourlot, J., Pineau des Forets, G., & Roueff, E. 2000, MNRAS, 314, 753

Fuller, T. M., & Couchman, H. M. P. 2000, ApJ, 544, 6

Galli, D., & Palla, F. 1998, A&A, 335, 403

Goldreich, P. & Kwan, J. 1974, ApJ, 189, 441

Haiman, Z., & Loeb, A. 1997, ApJ, 483, 21

Haiman, Z., & Loeb, A. 1998, ApJ, 503, 505

Haiman, Z., Rees, M. J., & Loeb, A. 1996, ApJ, 467, 522

Haiman, Z., Rees, M. J., & Loeb, A. 1997, ApJ, 476, 458

Heger, A., Woosley, S. E., & Waters, R. 2000, in The First Stars, eds. A. Weiss, T. Abel, & V. Hill, Springer, p.121

Henry, R. C., & Murthy, J. 1993, ApJ, 418, L17

Hernandez, X. & Ferrara, A. 2001, MNRAS, in press

Irwin, M., McMahon, R., & Hazard, C. 1991, ASP Conf. Ser. in The Space Distribution of Quasars, Vol. 21, 117

Kunth, D., & Sargent, W. L. W. 1986, ApJ, 300, 496

Larson, R. B. 1986, MNRAS, 218, 409

Larson, R. B. 1998, MNRAS, 301, 569

Lepp, S., & Shull, M. 1984, ApJ, 280, 465

Maloney, P. 1993, ApJ, 414, 41

Matsuda, T., Sato, H., & Takeda, H. 1969, Prog. Theor. Phys., 42, 219

McWilliam, A., Preston, G. W., Sneden, C., & Searle, L. 1995, AJ, 109, 2757

Nakamura, F., Hanawa, T., & Nakano, T. 1993, PASJ, 45, 551

Nakamura, F., & Umemura, M. 1999a, ApJ, 515, 239 (Paper I)

Nakamura, F., & Umemura, M. 1999b, in Star Formation 1999, ed. T. Nakamoto, Nobeyama Radio Observatory, p. 28

Nakamura, F., & Umemura, M. 2000, in The First Stars, eds. A. Weiss, T. Abel, & V. Hill, Springer, p. 263

Nakamura, F., & Umemura, M. 2001, ApJ, 548, 19 (Paper II)

Nakamura, T., Umeda, H., Iwamoto, K., Nomoto, K., Hashimoto, M., Hix, W. R., & Thielemann, F.-K. 2001, submitted to ApJ, (astro-ph/0011184)

Nishi, R. 2001, in The Physics of Galaxy Formation, p. 73

Nishi, R., Susa, H., Uehara, H., Yamada, M., & Omukai, K. 1998, Prog. Theor. Phys., 100, 881

Nishi, R., & Tashiro, M. 2000, ApJ, 537, 50

O'Meara, J. M., Tytler, D., Kirkman, D., Suzuki, N., Prochaska, J. X., Lubin, D., & Wolfe, A. M. 2001, accepted by ApJ(astro-ph/111790)

Omukai, K., & Nishi, R., 1998, ApJ, 508, 141

Omukai, K. 2000, ApJ, 534, 809

Palla, F., Salpeter, E. E., & Stahler, S. W., 1983, ApJ, 271, 632

Ryan, S. G., Norris, J. E., & Beers, T. C. 1996, ApJ, 471, 254

Pustilnik, S. A., Brinks, E., Thuan, T. X., Lipovetsky, V. A., & Izotov, Y. I. 2001, AJ, 121, 1413

Puy, D., Alecian, G., Lebourlot, J., Leorat, J., & Pineau des Forets, G., 1993, A&A, 267, 337

Puy, D., & Signore, M., 1996, A&A, 305, 371

Shapiro, P. R., & Kang, H. 1987, ApJ, 318, 32

Shigeyama, T., & Tsujimoto, T. 1998, ApJ, 507, L135

Stancil, P. C., Lepp, S. & Dalgarno, A. 1998, ApJ, 509, 1

Susa, H., Uehara, H., & Nishi, R. 1996, Prog. Theor. Phys., 96, 1073

Susa, H., Uehara, H., Nishi, R., & Yamada, M. 1998, Prog. Theor. Phys., 100, 63

Susa, H., & Umemura, M. 2000, ApJ, 537, 578

Tegmark, M., Silk, J., Rees, M., Blanchard, A., Abel, T., & Palla, F. 1997, ApJ, 474, 1

Tsuru, T. G., Awaki, H., Koyama, K., & Ptak, A. 1997, PASJ, 49, 619

Tytler, D., Fan, X.-M., & Burles, S. 1996, Nature, 381, 207

Yoneyama, T. 1972, PASJ, 24, 87

Yoshii, Y., & Sabano, Y. 1980, PASJ, 32, 229

Yoshii, Y., & Saio 1986, ApJ, 301, 587

Uehara, H., Susa, H., Nishi, R., & Yamada, M. 1996, ApJ, 473, L95

Uehara, H., & Inutsuka, S. 2000, ApJ, 531, L91

Umemura, M., Loeb, A., & Turner, E. 1993, ApJ, 419, 459

Umeda, H., & Nomoto, K. 2001, in The Physics of Galaxy Formation, p. 45

Umemura, M. 1993, ApJ, 406, 361

van den Bergh, S. 1962, AJ, 67, 486

Vazdekis, A., Casuso, E., Peletier, R. F., & Beckman, J. E. 1996, ApJ, 106, 307

Worthey, G., Faber, S. M. & Gonzales, J. J. 1992, ApJ, 598, 69

Worthey, G., Dorman, B.& Jones, L. A. 1996, AJ, 112, 948

Zepf, S. E. & Silk, J. 1996, ApJ, 466, 114

Table 1. REACTION RATE COEFFICIENTS

	Reactions	Rate Coefficients (cm^3s^{-1})
(D1)	$D^+ + e \rightarrow D + h\nu$	$k_{D1} = 3.6 \times 10^{-12}(T/300)^{-0.75}$
(D2)	$D + H^+ \rightarrow D^+ + H$	$k_{D2} = 3.7 \times 10^{-10}T^{0.28}\exp(-43/T)$
(D3)	$D^+ + H \rightarrow D + H^+$	$k_{D3} = 3.7 \times 10^{-10}T^{0.28}$
(D4)	$D + H \rightarrow HD + h\nu$	$k_{D4} = 1.0 \times 10^{-25}$
(D5)	$D + H_2 \rightarrow H + HD$	$k_{D5} = 9.0 \times 10^{-11}\exp(-3876/T)$
(D6)	$HD^+ + H \rightarrow H^+ + HD$	$k_{D6} = 6.4 \times 10^{-10}$
(D7)	$D^+ + H_2 \rightarrow H^+ + HD$	$k_{D7} = 2.1 \times 10^{-9}$
(D8)	$HD + H \rightarrow H_2 + D$	$k_{D8} = 3.2 \times 10^{-11}\exp(-3624/T)$
(D9)	$HD + H^+ \rightarrow H_2 + D^+$	$k_{D9} = 1.0 \times 10^{-9}\exp(-464/T)$
(D10)	$D + H^+ \rightarrow HD^+ + h\nu$	$k_{D10} = \mathrm{dex}[-19.38 - 1.523\log T + 1.118(\log T)^2 - 0.1269(\log T)^3]$
(D11)	$D^+ + H \rightarrow HD^+ + h\nu$	$k_{D11} = \mathrm{dex}[-19.38 - 1.523\log T + 1.118(\log T)^2 - 0.1269(\log T)^3]$
(D12)	$HD^+ + e \rightarrow H + D$	$k_{D12} = 7.2 \times 10^{-8}T^{-1/2}$
(D13)	$D + e \rightarrow D^- + h\nu$	$k_{D13} = 3.0 \times 10^{-16}(T/300)^{0.95}\exp(-T/9320)$
(D14)	$D^+ + D^- \rightarrow 2D$	$k_{D14} = 5.7 \times 10^{-8}(T/300)^{-0.5}$
(D15)	$H^+ + D^- \rightarrow D + H$	$k_{D15} = 4.6 \times 10^{-8}(T/300)^{-0.5}$
(D16)	$H^- + D \rightarrow H + D^-$	$k_{D16} = 6.4 \times 10^{-9}(T/300)^{0.41}$
(D17)	$D^- + H \rightarrow D + H^-$	$k_{D17} = 6.4 \times 10^{-9}(T/300)^{0.41}$
(D18)	$D^- + H \rightarrow HD + e$	$k_{D18} = 1.5 \times 10^{-9}(T/300)^{-0.1}$

Note. — GP98: Galli & Palla (1998); SLD98: Stancil, Lepp, & Dalgarno (1998)

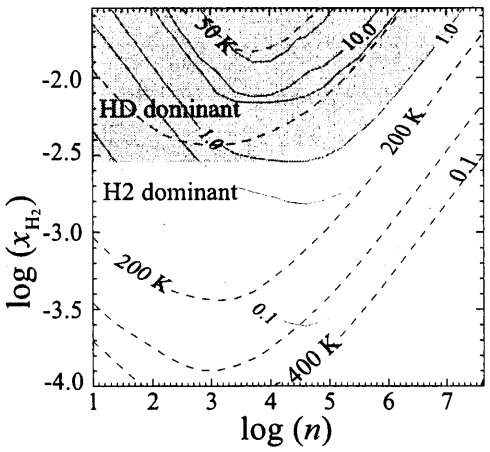

Fig. 1.— Comparison between the HD cooling rate and H_2 cooling rate. The figures show the ratios of the HD cooling rate to the H_2 cooling rate in the $n_0 - x_{H_2}$ plane for the models with $x_{HD}/x_{H_2} = 1 \times 10^{-4}$. The abscissa and ordinate indicate the cloud density and the initial H_2 abundance, respectively. The solid lines show the contour curves of the ratio of the HD to H_2 cooling rates, where the equilibrium gas temperatures are determined by the condition of $2.5t_{frag} = t_{cool}$ and are indicated by dashed lines. In this figure, an evolutionary path of a gravitationally collapsing cloud is nearly parallel to the abscissa because the H_2 abundance stays nearly constant during the contraction before the three-body reactions become important. For the filaments with $n_0 \lesssim 10^5$ cm^{-3} and $x_{H_2} \lesssim x_{H_2,cr}$, $\Lambda_{HD} < \Lambda_{H_2}$ during the contraction. For the filaments with $n_0 \lesssim 10^5$ cm^{-3} and $x_{H_2} \gtrsim x_{H_2,cr}$, the evolutionary path enters into the region of $\Lambda_{HD} > \Lambda_{H_2}$ in the course of contraction even if H_2 cooling is more efficient than HD cooling at the early stages. When the density exceeds 10^5 cm^{-3}, the contraction of the filaments slows down, and then, the actual temperature stays below 100 K. Consequently, HD cooling continues to play an important role in the contraction until the cloud becomes opaque to the HD lines. On the other hand, for the filaments with $n_0 \gtrsim 10^5$ cm^{-3} and $x_{H_2} \gtrsim x_{H_2,cr}$, the evolutionary path goes into the region of $\Lambda_{HD} < \Lambda_{H_2}$ even if Λ_{HD} is larger than Λ_{H_2} at the initial state. If the initial parameters of the filaments are in the gray region, the HD cooling plays an important role in the thermal evolution of the gas.

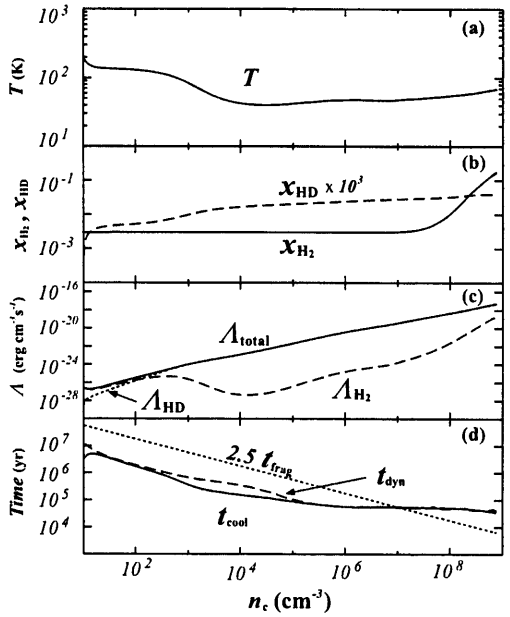

Fig. 2.— Evolution of (a) the temperature, (b) H_2 (*solid line*) and HD (*dashed line*) abundances, and (c) total (*solid line*), H_2 (*dashed line*), and HD (*dotted line*) cooling rates, (d) the cooling time (*solid line*), the contraction time (*dashed line*), and the fragmentation time (*dotted line*), respectively, as a function of the central density [$n_c \equiv \rho_c/(\mu m_H)$] for the model with $(n_0, T_0, f, x_{H_2,0}) = (10\,\mathrm{cm}^{-3},\ 200\,\mathrm{K},\ 2,\ 3\times10^{-3})$.

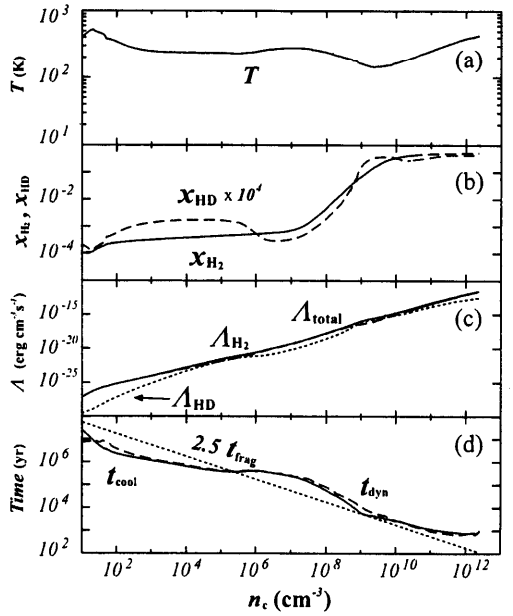

Fig. 3.— Same as Figure 2 but for the model with $(n_0, T_0, f, x_{H_2,0}) = (10\,\mathrm{cm}^{-3},\ 400\,\mathrm{K},\ 2,\ 1\times10^{-4})$.

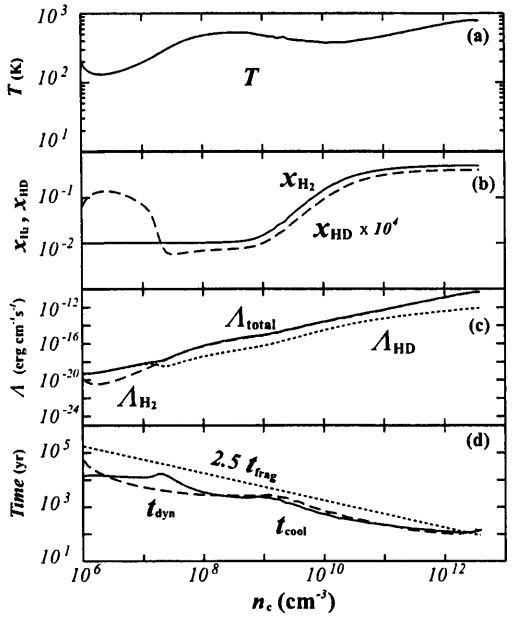

Fig. 4.— Same as Figure 2 but for the model with $(n_0, T_0, f, x_{H_2,0}) = (10^6\,\mathrm{cm}^{-3},\ 200\,\mathrm{K},\ 6,\ 1\times10^{-2})$.

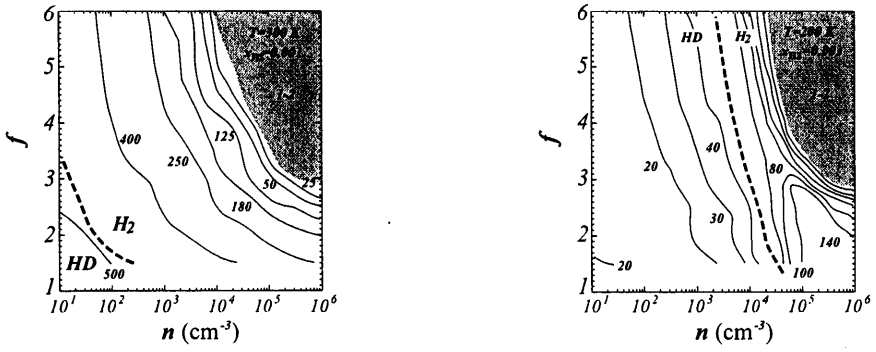

Fig. 5.— Mass distributions of fragments for the models with (a) 1×10^{-3} and (b) 3×10^{-3}. The abscissa and ordinate denote the initial central density and the parameter f, respectively. The solid lines denote the contours of the fragment mass which are labeled with adjacent numbers. The dashed lines show the lines at which the HD cooling rate is equal to H_2 cooling rate at the epoch of fragmentation. In the left regions of the dashed lines, HD cooling is more efficient than H_2 cooling.